JOURNAL OF ASIAN CERAMIC SOCIETIES
2021, VOL. 9, NO. 3, 1038–1045
https://doi.org/10.1080/21870764.2021.1935122

Characterization and separation resistance of an in-situ 2D nanocarbon/calcium aluminate composite synthesized via a combustion method

Shoulei Yang[a,b], Guoqing Xiao[c] and Donghai Ding[c]

[a]School of Materials Science and Engineering, Zhengzhou University of Aeronautics, Zhengzhou, China; [b]State Key Laboratory of Green Building in Western China, Xian University of Architecture and Technology, Xi'an, China; [c]College of Materials Science and Engineering, Xi'an University of Architecture and Technology, Xi'an, China

ABSTRACT

In-situ 2D nanocarbon/calcium aluminate composite (NCAC) was synthesized via a combustion method designed based on aluminothermic reduction using calcium carbonate ($CaCO_3$) as carbon source. The results demonstrate that compared with the pristine product, when the molar substitution rate of $CaCO_3$ for CaO_2 in the reactants was 25%, the contents of $CaAl_2O_4$ (CA), $CaAl_4O_7$ (CA_2) and $Ca_{12}Al_{14}O_{33}$ ($C_{12}A_7$) in the combusted product did not change substantially and were close to those of Secar71. When the molar substitution rate was increased to 50%, the contents of CA and CA_2 decreased, and that of $C_{12}A_7$ increased substantially. Interestingly, the nanocarbons generated in-situ in the combusted composite were embedded in calcium aluminate and had a nanoflake morphology (2D) with a thickness of approximately 50 nm, few defects and high graphitization degree. The results of the suspension experiment demonstrate that the floating ratio of NCAC in the suspension after ultrasonic vibration for 10 min was approximately 5.5 wt.%, which is much lower than that (78.8 wt.%) of a carbon black/Secar71 composite powder; thus, the in-situ 2D nanocarbon/aluminate composite had strengthened interfacial bonds and satisfactory separation resistance. These would be favorable for the uniform dispersion of nanocarbons within the matrix, improving the performance of cement-based composites.

ARTICLE HISTORY
Received 5 January 2021
Accepted 23 May 2021

KEYWORDS
Combustion synthesis; calcium aluminate; in-situ nanocarbon; separation resistance

1. Introduction

Due to their satisfactory electrical and thermal conductivities and high strength, nanocarbon (carbon nanotubes (CNTs), nanofiber (CNF) and graphene) modified cement-based composite materials (NMCs) are considered among the most promising candidates for civil engineering applications, such as structural monitoring and electromagnetic wave shielding [1–7]. However, one of the largest obstacles that restricts the practical application of these materials is the poor dispersion and low separation resistance of nanocarbons in the matrix due to their hydrophobic characteristics, large specific surface area and weak interfacial bonds [8,9].

In recent decades, physical methods (ultrasonication and ball milling), chemical methods (dispersants and chemical surface treatment) and combinations of physical and chemical methods have been utilized to improve the dispersion of nanocarbons in cement-based composites [10–16]. Although highly satisfactory results were obtained via these methods, many problems were encountered, such as deterioration of the microstructure and functionality of the nanocarbons, incompatibility with cement [10,17,18], influence of the cement hydration [6,19] and long time and high energy requirements [10]. These factors hinder the development and application of NMCs.

Recently, researchers proposed methods of in-situ growth of CNTs/CNFs on cement/mineral/silica fume particles via chemical vapor deposition (CVD) to improve the dispersion of nanocarbons in NMCs [20–23]. For example, Nasibulin *et al*. used the CVD method to grow CNTs and CNFs in-situ on sulfate-resistant cement and found that a hardened paste that was made from in-situ CNTs/CNFs cement had more than two times the compressive strength of pristine cement paste and showed a 70-fold increase in electrical conductivity [24]. Ludvig *et al.* report that CNTs/CNFs were grown in-situ on the surfaces of cement clickers and silica fume via the CVD method. Compared with pristine cement mortar, the tensile strength, flexural strength and compressive strength of cement mortar with the addition of in-situ CNTs/CNFs-cement clicker/silica fume were increased by 34.28%, 14.1% and 88.3%, respectively [22,25].

The methods for the in-situ growth of nanocarbons on the surfaces of cement//mineral/silica fume particles via CVD have advantages in maintaining the structural integrity of nanocarbons and improving interfacial bonds and are considered among the most suitable processes for improving the dispersion of nanocarbons in NMCs. However, these methods

CONTACT Shoulei Yang yanglei20080807@163.com

require flammable and explosive gases (such as CH_4 and H_2), which escalates the risk factors that are associated with the process. Additionally, due to the accumulation of the particles during the CVD process, the in-situ nanocarbons can only grow on the surfaces of the accumulations, which results in inhomogeneous growth of the in-situ nanocarbons in the powders. Development of more effective dispersion technologies is still attractive.

Herein, we present the synthesis of an in-situ nanocarbon/calcium aluminate composite (NCAC) via a combustion method that was designed based on a thermite reaction in which carbonate is used as a carbon source. In contrast to the CVD process, which consumes flammable and explosive gases directly, CO_2 gas that originates from the decomposition of carbonate during the process of combustion synthesis acts as a carbon source for the formation of in-situ nanocarbons. The combustion method has been applied to the synthesis of aluminate cement [26–31] and nanocarbon materials [32,33]. Therefore, the synthesis of in-situ nanocarbon/aluminate composites via the combustion method is feasible.

In the present study, NCAC was synthesized via a combustion method with calcium carbonate ($CaCO_3$) as the carbon source and aluminum (Al), alumina (Al_2O_3) and calcium peroxide (CaO_2) as raw materials. The separation resistance of the synthesized in-situ nanocarbon/aluminate composite in water was evaluated.

2. Experimental

As raw materials, calcium peroxide powder (CaO_2, particle size <25 μm), calcium carbonate powder ($CaCO_3$, particle size <25 μm), aluminum powder (Al, particle size 2~3 μm) and alumina powder (Al_2O_3, particle size <74 μm) of analytical purity were purchased from Sinopharm Chemical Reagent (Shanghai) Co. Ltd. A previous study reported that the phase compositions of the combusted product were equal to those of commercial Secar71 when the molar ratio of CaO/Al_2O_3 (C/A) in the ratio of raw materials CaO_2, Al and Al_2O_3 was 0.8 [30]. Therefore, aiming at the combustion synthesis of in-situ nanocarbon/aluminate composites with similar phase compositions to commercial Secar71, the C/A molar ratio was fixed at 0.8 in the present study, and $CaCO_3$ was used as a carbon and calcium source to partially replace CaO_2. The considered reaction can be expressed by Equation (1). The *r* value is the molar substitution coefficient of $CaCO_3$ for CaO_2.

$$(1-r)CaO_2 + rCaCO_3 + 0.66(1+r)Al + (0.87 - 0.33r)Al_2O_3 = 0.75CaAl_2O_4 + 0.25CaAl_4O_7 + rC \quad (1)$$

The starting reactants were weighed according to Table 1 and mixed in a ball mill for 40 min. The well-mixed reactants were then placed in a quartz crucible, and buried with a Ti-C powder at a molar ratio of 1:1. After that, the quartz crucible was placed in a combustion synthesis reactor. The combustion reaction was ignited with the Ti-C powder and proceeded in an argon atmosphere at a pressure of 0.1 MPa. A schematic diagram of the combustion synthesis of NCAC is shown in Figure 1.

Table 1. Raw material ratios and substitution coefficients (*r*).

Samples	*r*	Mass fraction (wt.%)			
		$CaCO_3$	CaO_2	Al_2O_3	Al
CA-0.8–0.00	0.00	0.00	39.24	50.95	9.81
CA-0.8–0.25	0.25	13.40	28.95	45.58	12.06
CA-0.8–0.50	0.50	26.39	19.00	40.37	14.25

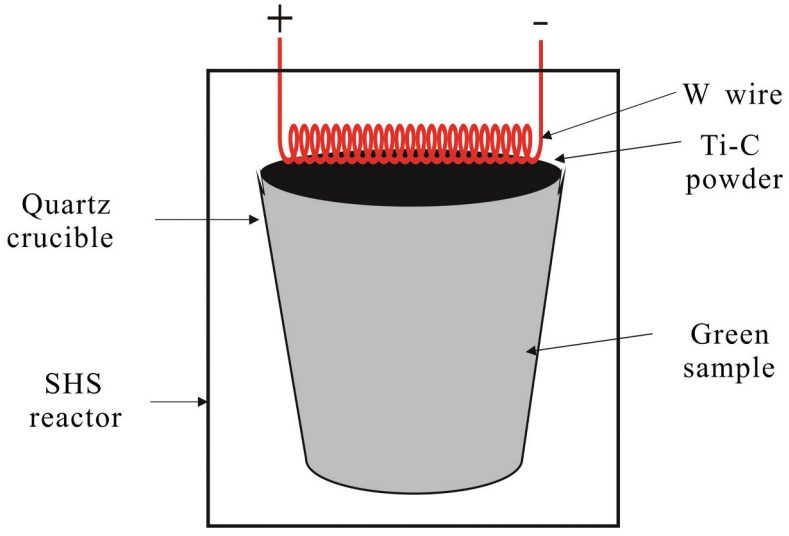

Figure 1. A schematic diagram of the combustion synthesis of NCAC.

The phase of the combusted product was identified via X-ray diffraction (XRD, D/MAX 2400, Japan) with Cu K radiation (λ = 1.5406 Å) at a scanning speed of 5°/min. The morphologies were observed with a field-emission scanning electron microscope that was equipped with an energy-dispersive spectrometer (FESEM-EDS, SU6600, Japan). The nanocarbon that was generated in-situ in the product was characterized via Raman spectroscopy (Renishaw-Invia), high-resolution transmission electron microscopy (HRTEM, FEI Tecnai G2 F20, USA) and infrared carbon-sulfur analysis (HCS-140).

Based on a suspension method that is described in the literature [34–36], the separation resistance of the in-situ nanocarbon/aluminate composite in water was evaluated. Twenty grams of the synthesized composite powder and 200 ml deionized water were placed in a beaker and ultrasonically vibrated for 10 min. A photograph of the suspension after being set aside for 30 min was captured. The floating materials were separated from the suspension and dried in a vacuum oven at 80°C for 12 h. The floating ratio (FR, wt.%) was calculated according to Equation (2). A lower FR value corresponds to a higher separation resistance. For comparison, a suspension of a carbon black/Secar71 composite powder (which was prepared by mechanically mixing carbon black with Secar71 and labeled S71CB) was also prepared and tested according to the above method.

$$FR(\%) = \frac{FW}{OW} \times 100\% \quad (2)$$

where FR (%) denotes the floating ratio, FW denotes the weight of the floating materials (g) and OW denotes the weight of the original carbon in the composite (g).

3. Results and discussion

3.1. Characterizations of NCAC

Figure 2(a) shows the full XRD patterns of the combusted products, according to which the products were composed of mayenite ($Ca_{12}Al_{14}O_{33}$, $C_{12}A_7$), monocalcium aluminate ($CaAl_2O_4$, CA) and calcium

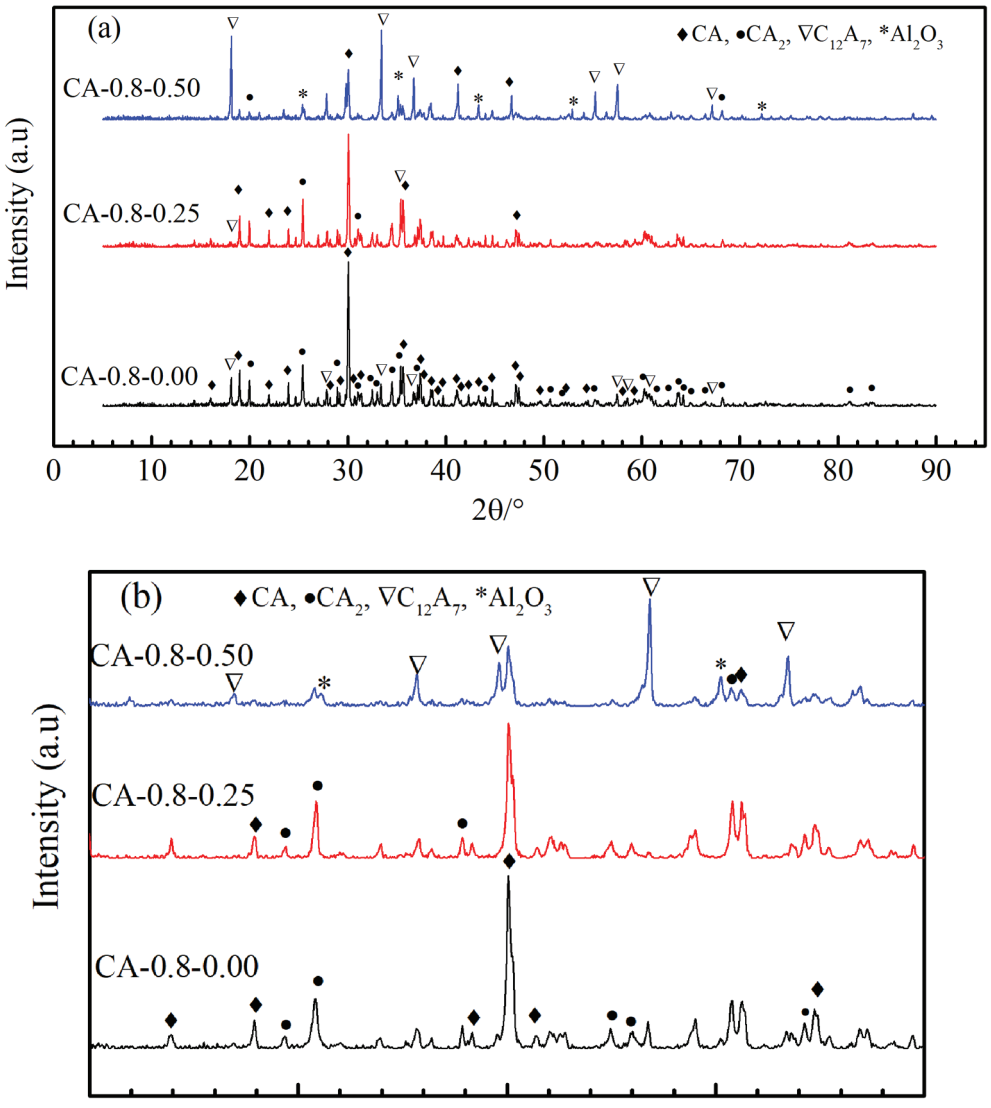

Figure 2. (a) Full XRD patterns of the synthesized composites. (b) Local amplification of XRD patterns.

dialuminate ($CaAl_4O_7$, CA_2). According to the local amplifications of the XRD patterns, as shown in Figure 2(b), when the molar substitution rate of CaO_2 by $CaCO_3$ was 25%, the main characteristic peaks at 30.140°, 25.407° and 33.425°, which correspond to CA, CA_2 and $C_{12}A_7$, respectively, were similar to those of the C/A-0.8–0.00 sample; thus, the contents of CA, CA_2 and $C_{12}A_7$ in the C/A-0.8–0.25 sample did not vary substantially. These results are supported by quantitative results for the components that were obtained using the XRD-Rietveld method, which are presented in Table 2. In addition, the phase compositions of the C/A-0.8–0.25 sample were close to those of Secar71. When the molar substitution rate of $CaCO_3$ was increased to 50%, the main characteristic peaks of CA and CA_2 in the XRD pattern of the CA-0.8–0.50 sample decreased, those of $C_{12}A_7$ substantially increased, and the characteristic peaks of the residual Al_2O_3 appeared. The contents of CA and CA_2 in the CA-0.8–0.5 sample decreased to 54.45 wt.% and 8.78 wt.%, respectively, and that of $C_{12}A_7$ increased to 24.56 wt.%.

The adiabatic temperatures (T_{ad}) of the CaO_2-Al-Al_2O_3-$CaCO_3$ system for the combustion synthesis of NCAC were calculated based on thermodynamic data from the literature [37,38], and the results are presented in Figure 3. As the molar substitution rate of $CaCO_3$ for CaO_2 increased from 0% to 50%, the T_{ad} values decreased from 2895 to 1855 K. The combustion temperatures showed a similar variation trend. These effects were adverse for the transformation of $C_{12}A_7$ (which was usually generated first as a metastable phase) into CA and CA_2 [31,39]. Therefore, the contents of CA and CA_2 in the combusted product decreased with the molar substitution of $CaCO_3$ for CaO_2, whereas that of $C_{12}A_7$ increased.

Table 2. Relative contents of CA, CA_2 and $C_{12}A_7$ in the combustion product.

Samples	Contents (wt.%)		
	CA	CA_2	$C_{12}A_7$
CA-0.8–0.00	62.55	33.40	0.68
CA-0.8–0.25	61.82	34.94	0.45
CA-0.8–0.50	54.45	8.78	24.56
Secar71	60.25	35.45	0.5

In contrast to the pristine product, the products that were synthesized with $CaCO_3$ as a reactant were black. Therefore, Raman spectroscopy, which is an effective technology for characterizing carbon materials, was used to characterize the combusted products, and the results are presented in Figure 4. In contrast to the spectrum of CA-0.8–0.00, in the CA-0.8–0.25 and CA-0.8–0.50 spectra, three distinct bands are observed at 1350 cm^{-1}, 1580 cm^{-1}, and 2700 cm^{-1}, which are ascribed to the D, G, and 2D bands, respectively, of carbon materials. The D band at approximately 1350 cm^{-1}, of which the intensity increased as the graphitization degree of the carbon material decreased, is associated with defects. The G band, located at approximately 1580 cm^{-1}, is a typical feature of all graphitic materials. The band at approximately 2700 cm^{-1} (2D) can be used to evaluate the number of layers of few-layer graphene [40]. The ratio of the intensities of the D and G bands (I_D/I_G) can be used as an indicator of the graphitization degree of the carbon materials, where a smaller I_D/I_G value indicates higher graphitic ordering [41]. The I_D/I_G values of the CA-0.8–0.25 and CA-0.8–0.50 spectra were calculated and are listed in Table 3. The I_D/I_G values were approximately 0.28 and 0.31, respectively. These results demonstrate that carbon materials of high graphitization degree were generated in-situ in the CA-0.8–0.25 and CA-0.8–0.50 samples. Their carbon contents were 0.86 wt.% and 1.27 wt.%, respectively.

The fracture surfaces of the CA-0.8–0.25 and CA-0.8–0.00 samples were observed via FESEM, and the results are shown in Figure 5. Figure 5(a) shows that many pore structures with various diameters appeared in the CA-0.8–0.25 sample due to the generation of gases during the process of combustion synthesis.

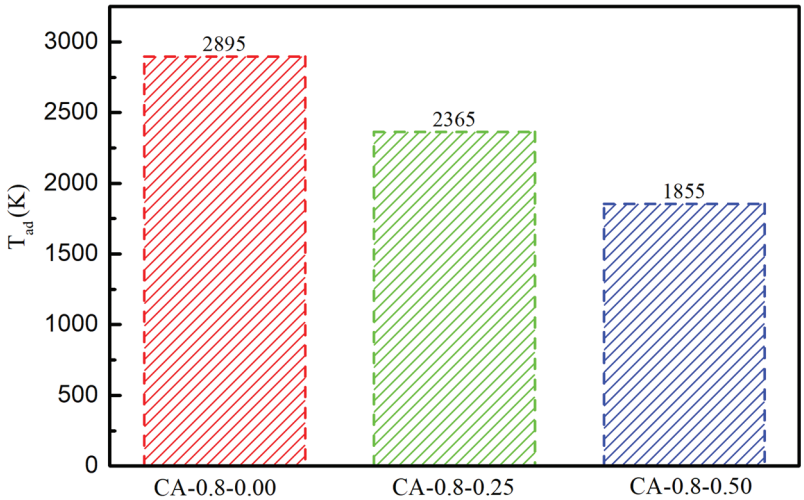

Figure 3. The adiabatic temperatures (T_{ad}) of the CaO_2-Al-Al_2O_3-$CaCO_3$ system.

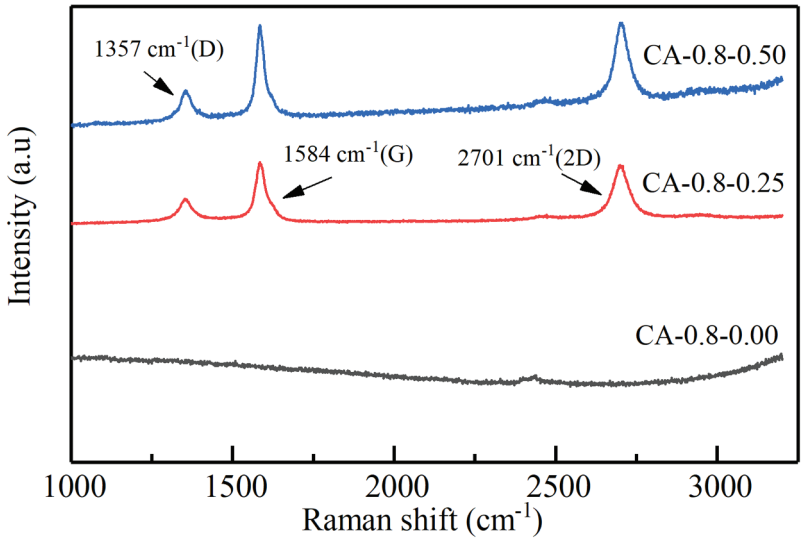

Figure 4. Raman patterns of the combusted products.

Table 3. In-situ nanocarbon contents and I_G/I_D ratios of the products.

Samples	Carbon contents (wt.%)	I_D/I_G ratio
CA-0.8–0.00	0.00	-
CA-0.8–0.25	0.86	0.28
CA-0.8–0.50	1.27	0.31

Figure 5(b), which corresponds to the red hole in Figure 5(a), shows that the microstructure of the CA-0.8–0.25 sample contains cubic and prismatic grains and is similar to that of the CA-0.8–0.00 sample (as shown in Figure 5(c)). From the relevant EDS and XRD results, it is inferred that "A", which represents the cuboid morphology with a molar ratio of Ca, Al, and O of approximately 1:2:4, was a CA grain and "B", which represents the prism morphology with a molar ratio of approximately 1:4:7, was a CA_2 grain. The microstructure was further examined by enlarging the blue square in Figure 5(a), and the results are shown in Figure 5(d). Interestingly, many nanoflakes are observed in the product. Enlarging the yellow square in Figure 5(d), Figure 5(e) clearly shows that nanoflakes with a thickness of approximately 50 nm were embedded in calcium aluminates. Based on the EDS results (as shown in Table 4) of the green square area in Figure 5(e), it is inferred that the nanoflakes were carbon materials, with similar morphologies to those reported in the literature [32,33].

To better characterize the nanocarbons that were generated in-situ in the combusted product, the CA-0.8–0.25 sample was further examined via HRTEM, and the results are shown in Figure 6. Figure 6(b), which corresponds to the red square in Figure 6(a), implies that the nanoflakes that are embedded in the calcium aluminate have a clear graphitic layer with an interplanar spacing of 0.339 nm, which corresponds well with the (002) plane of graphite; thus, the in-situ 2D nanocarbon that is generated in the combusted composite has a high graphitization degree. In addition, the interfacial bond between the in-situ nanocarbon and aluminate was strengthened.

3.2. Separation resistance of NCAC

The C/A-0.8–0.25 sample, which was similar in phase composition to Secar71, was ground into a powder and is denoted as NCAC. The specific surface areas of NCAC and S71CB, as determined via the BET method, were approximately 402 m^2/kg and 392 m^2/kg, respectively. The separation resistances of NCAC and S71CB in water were evaluated according to the suspension method. For the S71CB suspension, the weight of floating materials in the suspension was increased with ultrasonic time. When the S71CB suspension was ultrasonically vibrated for 10 min, the weight of floating materials in the S71CB suspension after being set aside for 30 min was maximum, and the results are presented in Figure 7.

According to Figure 7(a), many black materials were floating on the S71CB suspension after the sample was ultrasonically vibrated for 10 min and set aside for 30 min, whereas this phenomenon was not readily observed in the NCAC suspension, as shown in Figure 7(b). The floating ratios (FR, %) of the two suspensions are presented in Figure 7(c). The FR value of the NCAC suspension was approximately 5.5%, which is substantially lower than that (78.8%) of the S71CB suspension, thence, the separation resistance of NCAC was higher than that of S71CB. These results can be attributed to the strengthened interfacial bonds of the in-situ 2D nanocarbons that are embedded in calcium aluminate and to the nanocarbons being surrounded by hydrophilic species (AH_3, CAH_{10}, C_2
AH_8 and C_3AH_6) from the hydration of calcium aluminates, thereby preventing the separation of the nanocarbons from the matrix.

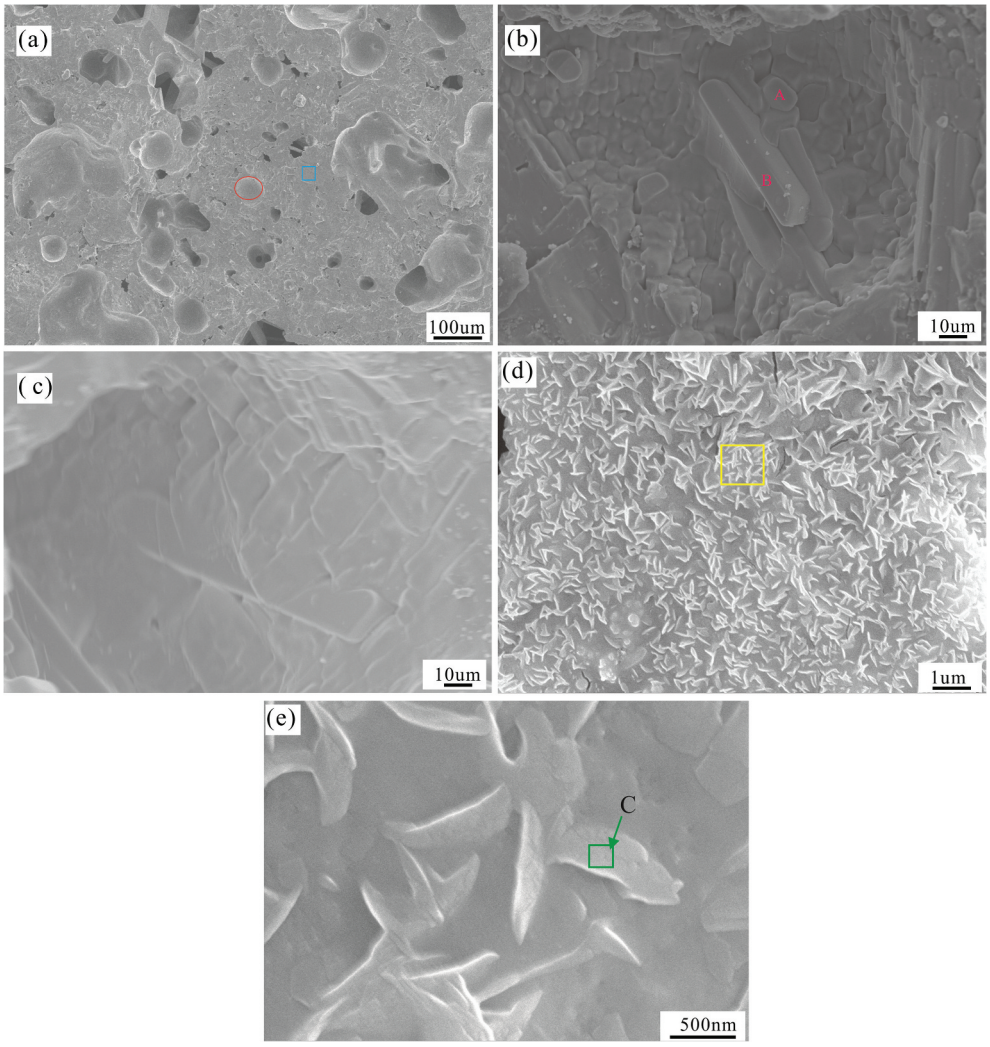

Figure 5. FESEM images of the combustion products. (a, b, d, e) $r = 0.25$; (c) $r = 0.00$.

Table 4. The EDS results of A, B and C areas in Figure 5.

Points	*Wt.*%				*At.* %			
	C	O	Al	Ca	C	O	Al	Ca
A	/	23.86	44.38	31.76	/	37.97	41.86	20.17
B	/	40.03	43.61	16.36	/	55.27	35.71	09.02
C	44.54	07.71	25.80	17.18	66.23	08.60	17.08	07.66

The dispersion state of the nanocarbons within the matrix directly affects the mechanical properties and functional properties of NMCs [8,9]. Usually, nanocarbon materials were separated from the matrix due to their low density and weak interfacial bonding during the preparation of NMCs, thereby resulting in poor dispersion in the NMCs. Thus, the satisfactory separation resistance of the in-situ nanocarbon/aluminate composite would improve the dispersion of nanocarbons in the matrix, thereby producing cement-based composite materials with high performance. Furthermore, the mechanical and functional properties of NMCs with NCAC as a binder are currently being investigated.

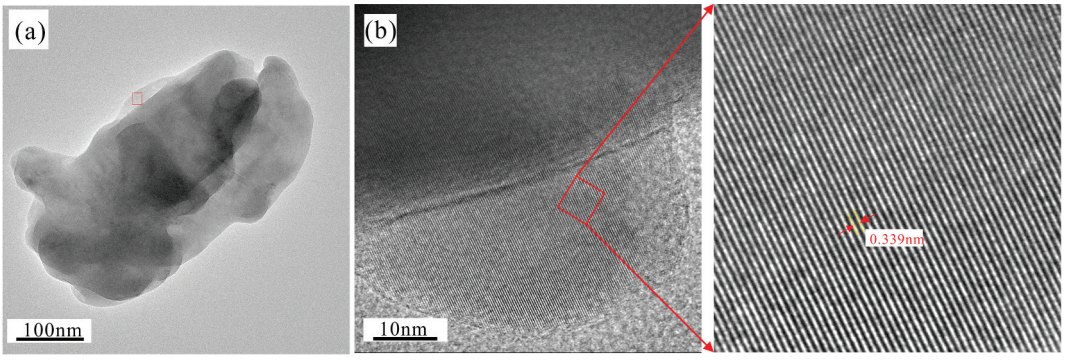

Figure 6. (a) TEM image of the sample CA-0.8–0.25; (b) HRTEM image of the sample CA-0.8–0.25.

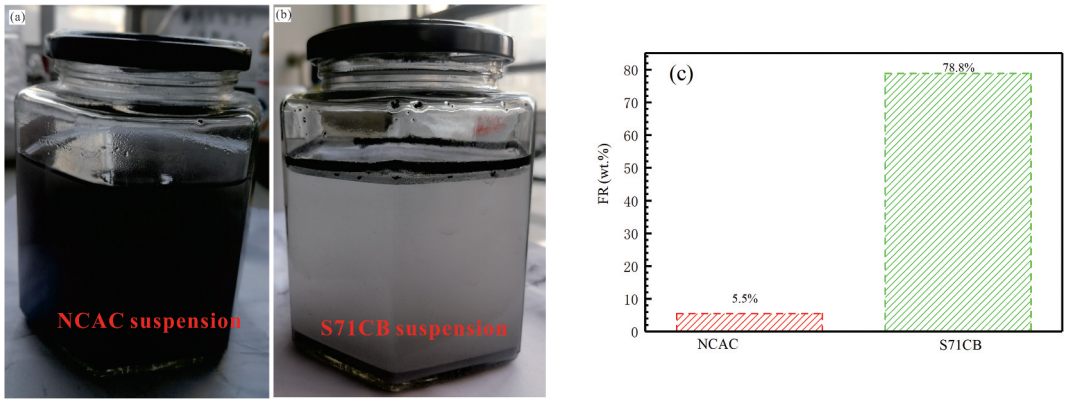

Figure 7. (a, b) The photographs of the NCAC and S71CB suspensions after being ultrasonically vibrated. (c) The floating ratios of the NCAC and S71CB suspensions.

4. Conclusions

An in-situ 2D nanocarbon/calcium aluminate composite with a similar phase composition to commercial Secar71 was successfully prepared via a combustion method by adjusting the molar substitution ratio of $CaCO_3$ for CaO_2 in the raw reactants. The 2D nanocarbons that were generated in-situ in the combusted product had a thickness of approximately 50 nm, few defects and a high graphitization degree and were embedded in aluminates. The low floating ratio of NCAC in the suspension implied that the in-situ 2D nanocarbon/calcium aluminate composite had increased separation resistance, which would be favorable for the uniform dispersion of nanocarbons in NMCs and would enhance their properties. These results suggest that the synthesis of in-situ nanocarbon/calcium aluminate composites via this combustion method would be an effective and promising approach for the preparation of nanocarbon-modified cement-based composites.

Acknowledgments

This work was supported by the Opening Fund of State Key Laboratory of Green Building in Western China (No. LSKF202006), Key Science and Technology Program of Henan (No. 202102210019) and the National Natural Science Foundation of China (No. 51772236).

Disclosure of potential conflicts of interest

No potential conflict of interest was reported by the author(s).

Funding

This work was supported by the National Natural Science Foundation of China [51772236]; the Opening Fund of State Key Laboratory of Green Building in Western China [LSKF202006]; Key Science and Technology Program of Henan [202102210019].

References

[1] Reales O, Filho R. A review on the chemical, mechanical and microstructural characterization of carbon nanotubes-cement based composites. Constr Build Mater. 2017;154(15):697–710.
[2] Xu J, Zhang D. Pressure-sensitive properties of emulsion modified graphene nanoplatelets/cement composites. Cem Concr Compos. 2017;84:74–82.
[3] Shi T, Li Z, Guo J, *et al*. Research progress on CNTs/CNFs-modified cement-based composites: a review. Constr Build Mater. 2019;202(30):290–307.
[4] Monteiro A, Cachim P, Costa P. Self-sensing piezoresistive cement composite loaded with carbon black particles. Cem Concr Compos. 2017;81:59–65.
[5] Jung M, Lee Y, Hong S, *et al*. Carbon nanotubes (CNTs) in ultra-high-performance concrete (UHPC): dispersion, mechanical properties, and electromagnetic interference (EMI) shielding effectiveness (SE). Cem Concr Res. 2020;131:106017–106032.
[6] Wei J, Fan Y, Zhao L, *et al*. Thermoelectric properties of carbon nanotube reinforced cement-based composites fabricated by compression shear. Ceram Int. 2018;44(6):5829–5833.
[7] Singh A, Gupta B, Mishr M, *et al*. Multiwalled carbon nanotube/cement composites with exceptional electromagnetic interference shielding properties. Carbon. 2013;56:86–96.
[8] Liew K, Kai M, Zhang L. Carbon nanotube reinforced cementitious composites: an overview. Compos Part A. 2016;91:301–323.
[9] Han B, Sun S, Ding S. Review of nanocarbon-engineered multifunctional cementitious composites. Compos Part A. 2015;70:69–81.
[10] Grossiord N, Regev O, Loos J, *et al*. Time-dependent study of the exfoliation process of carbon nanotubes in aqueous dispersions by using UV-visible spectroscopy. Anal Chem. 2005;77(16):5135–5139.
[11] Ubertini F, Materazzi A, Alessandro A, *et al*. Natural frequencies identification of a reinforced concrete beam using carbon nanotube cement-based sensors. Eng Struct. 2014;60:265–275.
[12] Lu K, Lago R, Chen Y, *et al*. Mechanical damage of carbon nanotubes by ultrasound. Carbon. 1996;34(6):814–816.

[13] Shao H, Chen B, Li B, *et al*. Influence of dispersants on the properties of CNTs reinforced cement-based materials. Constr Build Mater. 2017;131(30):186–194.
[14] Li G, Wang P, Zhao X. Mechanical behavior and microstructure of cement composites incorporating surface-treated multi-walled carbon nanotubes. Carbon. 2005;43(6):1239–1245.
[15] Datsyuk V, Kalyva M, Papagelis K, *et al*. Chemical oxidation of multiwalled carbon nanotubes. Carbon. 2008;46(6):833–840.
[16] Peyvandi A, Soroushiana P, Abdol N, *et al*. Surface-modified graphite nanomaterials for improved reinforcement efficiency in cementitious paste. Carbon. 2013;63:175–186.
[17] Yazdanbakhsh A, Grasley Z, Tyson B, *et al*. Carbon nano filaments in cementitious materials: some issues on dispersion and interfacial bond. Special Publication; 2009. p. 21–34.
[18] Brown L, Sanchez F. Influence of carbon nanofiber clustering on the chemo-mechanical behavior of cement pastes. Cem Concr Compos. 2016;65:101–109.
[19] Ma P, Kim J, Tang B. Effects of silane functionalization on the properties of carbon nanotube/epoxy nanocomposites. Compos Sci Technol. 2007;67 (14):2965–2972.
[20] Mudimela P, Nasibulina L, Nasibulin A, *et al*. Synthesis of carbon nanotubes and nanofibers on silica and cement matrix materials. J Nanomater. 2009;1–4.
[21] Nasibulin A, Koltsova T, Nasibulina L, *et al*. A novel approach to composite preparation by direct synthesis of carbon nanomaterial on matrix or filler particles. Acta Materialia. 2013;61(6):1862–1871.
[22] Sun S, Xu Y, Han B, *et al*. In situ growth of carbon nanotubes/carbon nanofibers on cement/mineral admixture particles: a review, Constr. Build Mater. 2013;49:835–840.
[23] Zhang X, Liu Z. Recent advances in microwave-initiated synthesis of nanocarbon materials. Nanoscale. 2012;4(3):707–714.
[24] Nasibulin A, Shandakov S, Nasibulina L, *et al*. A novel cement-based hybrid material. New J Phys. 2009;11:023013.
[25] Ludvig P, Calixto J, Ladeira L, *et al*. Using converter dust to produce low-cost cementitious composites by in situ carbon nanotube and nanofiber synthesis. Materials. 2011;4:575–584.
[26] Ianoş R, Lazău I, Păcurariu C, *et al*. Fuel mixture approach for solution combustion synthesis of $Ca_3Al_2O_6$ powder. Cem Concr Res. 2009;39:566–572.
[27] Fumo D, Morelli M, Segadães A. Combustion synthesis of calcium aluminates. Mater Res Bull. 1996;31 (10):1243–1255.
[28] Burkes D, Moore J. Auto-ignition combustion synthesis of calcium aluminate ceramic powders. Combust Sci Technol. 2008;180(1):143–155.
[29] Cüneyt Tas A. Chemical preparation of the binary compounds in the calcia-alumina system by self-propagating combustion synthesis. J Am Ceram Soc. 1998;81(11):2853–2863.
[30] Yang S, Xiao G, Ding D, *et al*. Preparation of calcium aluminate cement by combustion synthesis and application for corundum based castables. Int J Appl Ceram Technol. 2018;15(3):678–688.
[31] Yang S, Xiao G, Ding D, *et al*. Dissolution-precipitation mechanism of combustion synthesis of calcium aluminate. Ceram Int. 2017;43(17):159818.
[32] Dabrowska A, Huczko A, Soszynski M, *et al*. Ultra-fast efficient synthesis of one-dimensional nanostructures. Phys Status Solidi B. 2011;248(11):2704–2707.
[33] Dabrowska A, Huczko A, Dyjak S. Fast and efficient combustion synthesis route to produce novel nanocarbons. Phys Status Solidi B. 2012;249 (12):2373–2377.
[34] Zhang S, Lee W. Improving the water-wettability and oxidation resistance of graphite using Al_2O_3/SiO_2 sol-gel coatings. J Eur Ceram Soc. 2003;23 (8):1215–1221.
[35] Yoshimatsu H, Fujiwara S, Konishi R, *et al*. Wettability by water and oxidation resistance of alumina-coated graphite powder. J Ceram Soc Jpn. 1995;103 (1201):929–934.
[36] Xiao G, Yang S, Ding D, *et al*. One-step synthesis of in-situ carbon containing calcium aluminae cement as binders for refractory castables. Ceram Int. 2018;44 (13):15378–15384.
[37] Rogachev A, Mukasyan A. Combustion for material synthesis. Boca Raton: CRC Press; 2014.
[38] Ye D, Hu J. Practical handbook of thermodynamic data for inorganic substances. 2nd ed. Beijing: Metallurgical Industry Press; 2002.
[39] Yang S, Xiao G, Ding D, *et al*. Thermodynamic analysis of combustion synthesis of calcium aluminate in CaO-Al-Al_2O_3-$CaCO_3$-O_2 system. J Chin Ceram Soc. 2016;44(6):908–913.
[40] Malard L, Pimenta M, Dresselhaus G, *et al*. Raman spectroscopy in graphene. Phys Rep. 2009;473 (5–6):51–87.
[41] Ferrari A. Raman spectroscopy of graphene and graphite: disorder, electron–phonon coupling, doping and nonadiabatic effects. Solid State Commun. 2007;143(1–2):47–57.